




RESEARCH PAPER

Rare earth elements induce cytoskeleton-dependent and PI4P-associated rearrangement of SYT1/SYT5 endoplasmic reticulum–plasma membrane contact site complexes in Arabidopsis

EunKyung Lee¹, Brenda Vila Nova Santana^{1,2}, Elizabeth Samuels¹, Francisco Benitez-Fuente¹, Erica Corsi¹, Miguel A. Botella³, Jessica Perez-Sancho^{3,4}, Steffen Vanneste^{5,6,7}, Jiří Friml⁸, Alberto Macho⁴, Aristeia Alves Azevedo² and Abel Rosado^{1,*} 

¹ Department of Botany, University of British Columbia, Vancouver, V6T 1Z4, Canada

² Departamento de Biologia Vegetal, Universidade Federal de Viçosa, 36570-900 Viçosa, Minas Gerais, Brazil

³ Instituto de Hortofruticultura Subtropical y Mediterránea, Universidad de Málaga–Consejo Superior de Investigaciones Científicas (IHSM-UMA-CSIC), Departamento de Biología Molecular y Bioquímica, Universidad de Málaga, 29071 Málaga, Spain

⁴ Shanghai Center for Plant Stress Biology, CAS Center for Excellence in Molecular Plant Sciences, Shanghai Institute of Biological Sciences, Chinese Academy of Sciences, Shanghai, 201602 China

⁵ Department of Plant Biotechnology and Bioinformatics, Ghent University, Ghent, Belgium

⁶ Center for Plant Systems Biology, VIB, Ghent, Belgium

⁷ Ghent University Global Campus, Incheon 21985, Korea

⁸ Institute of Science and Technology (IST), Klosterneuburg, Austria

* Correspondence: abel.rosado@botany.ubc.ca

Received 6 August 2019; Editorial decision 5 March 2020; Accepted 13 March 2020

Editor: Christine Raines, University of Essex, UK

Abstract

In plant cells, environmental stressors promote changes in connectivity between the cortical endoplasmic reticulum (ER) and the plasma membrane (PM). Although this process is tightly regulated in space and time, the molecular signals and structural components mediating these changes in interorganelle communication are only starting to be characterized. In this report, we confirm the presence of a putative tethering complex containing the synaptotagmins 1 and 5 (SYT1 and SYT5) and the Ca²⁺- and lipid-binding protein 1 (CLB1/SYT7). This complex is enriched at ER–PM contact sites (EPCSs), has slow responses to changes in extracellular Ca²⁺, and displays severe cytoskeleton-dependent rearrangements in response to the trivalent lanthanum (La³⁺) and gadolinium (Gd³⁺) rare earth elements (REEs). Although REEs are generally used as non-selective cation channel blockers at the PM, here we show that the slow internalization of REEs into the cytosol underlies the activation of the Ca²⁺/calmodulin intracellular signaling, the accumulation of phosphatidylinositol-4-phosphate (PI4P) at the PM, and the cytoskeleton-dependent rearrangement of the SYT1/SYT5 EPCS complexes. We propose that the observed EPCS rearrangements act as a slow adaptive response to sustained stress conditions, and that this process involves the accumulation of stress-specific phosphoinositide species at the PM.

Keywords: Arabidopsis, calcium, cytoskeleton, endoplasmic reticulum (ER), ER–PM membrane contact sites, phosphoinositides, PI4P, plasma membrane (PM), rare earth elements, stress adaptation, synaptotagmins, SYT1/SYT5.

Introduction

A hallmark of eukaryotic cells is the establishment of physical interfaces that enable organelle to organelle direct communication. These interfaces, known as membrane contact sites (MCSs), serve as platforms for the control of essential cellular functions including metabolism, regulation of organelle dynamics, and stress signal integration (Helle *et al.*, 2013; Bravo-Sagua *et al.*, 2014; Prinz, 2014; Pérez-Sancho *et al.*, 2016a). In plants, the establishment of MCSs between the endoplasmic reticulum (ER) and different organelles is particularly important for the coordination of key physiological functions including lipid transfer (e.g. ER–mitochondria and ER–plastid contact sites; Xu *et al.*, 2008; Block and Jouhet, 2015; Fan *et al.*, 2015; Michaud *et al.*, 2016), intercellular communication (e.g. plasmodesmata; Uchiyama *et al.*, 2014; Levy *et al.*, 2015; Tilsner *et al.*, 2016; Ishikawa *et al.*, 2020), organelle distribution (e.g. ER–peroxisome, ER–plastid, and ER–Golgi contact sites; Andersson *et al.*, 2007; Sparkes *et al.*, 2009; Barton *et al.*, 2013), and the Ca²⁺-dependent regulation of stress responses [ER–plasma membrane (PM) contact sites (EPCSs); Schapire *et al.*, 2008; Yamazaki *et al.*, 2008; P. Wang *et al.*, 2014, 2016; Pérez-Sancho *et al.*, 2015; Kim *et al.*, 2016; Lee *et al.*, 2019).

In Arabidopsis, the dynamic arrangement of EPCSs is regulated by multiple families of EPCS components, namely synaptotagmins (SYTs), vesicle-associated membrane protein (VAMP)-associated proteins 27 (VAP27s), NETWORKED 3 (NET3C), and VAP-RELATED SUPPRESSORS OF TOO MANY MOUTHS (VSTs) (Pérez-Sancho *et al.*, 2015; Wang *et al.*, 2017). These EPCS components serve a number of well-characterized functions including the response to biotic and abiotic stressors (Schapire *et al.*, 2008; Yamazaki *et al.*, 2008; Uchiyama *et al.*, 2014; Lewis and Lazarovitch, 2015; Levy *et al.*, 2015; Pérez-Sancho *et al.*, 2015; Kim *et al.*, 2016; Lee *et al.*, 2019), the control of the interactions between the ER and the cortical cytoskeleton (P. Wang *et al.*, 2014, 2016; Siao *et al.*, 2016), and the activation of signal transduction events through the activation of receptor-like kinases (Ho *et al.*, 2016).

This study expands on existing research on the Arabidopsis SYT1, which is an EPCS tether that localizes in immobile cortical ER tubules, and docks the PM through Ca²⁺-dependent interactions between its C2 domains and negatively charged phospholipids (Schapire *et al.*, 2008; Yamazaki *et al.*, 2010; Pérez-Sancho *et al.*, 2015, 2016b; Ishikawa *et al.*, 2018). Genetic studies using *sytl* loss-of-function mutants have shown that SYT1 is required for the control of immune secretory pathways (Kim *et al.*, 2016), maintenance of the cortical ER stability (Siao *et al.*, 2016), the regulation of cell to cell communication (Lewis and Lazarowitz, 2010; Uchiyama *et al.*, 2014; Levy *et al.*, 2015; Ishikawa *et al.*, 2020), and the tolerance to ionic, mechanical, and freezing stresses (Schapire *et al.*, 2008; Yamazaki *et al.*, 2010; Pérez-Sancho *et al.*, 2015). To achieve such diverse functions, SYT1 establish interactions with elements of the exocytic soluble SNAREs (Kim *et al.*,

2016), phytosterol-binding proteins (Dalal *et al.*, 2016), and reticulin proteins (Kriechbaumer *et al.*, 2015).

Recent studies have partially elucidated SYT1's mechanism of action by showing it increases ER–PM connectivity by promoting the cytoskeleton-independent and phosphatidylinositol 4,5-bisphosphate [PI(4,5)P₂]-associated EPCS expansion (Lee *et al.*, 2019), and that SYT1-labeled ER tubules can be disrupted by pharmacologically decreasing the intracellular Ca²⁺ concentration (Ishikawa *et al.*, 2018). Despite these advances, many aspects including the specificity of the PI(4,5)P₂ signal as a trigger for EPCS expansion, and the dynamics of EPCS organization in response to extracellular Ca²⁺ depletion remain largely unexplored.

In this study, we corroborate a recent report describing the establishment of a putative tethering complex between the synaptotagmins 1 and 5, and the Ca²⁺-dependent lipid binding protein CLB1/SYT7 (hereafter CLB1) at EPCSs (Ishikawa *et al.*, 2020), and we expand their analysis by showing that SYT1 and SYT5 can form homo- and heterodimers *in vivo*. We also show that changes in extracellular Ca²⁺ have a limited effect in EPCS organization with the exception of treatments with salts of the rare earth elements (REEs) lanthanum (La³⁺) and gadolinium (Gd³⁺). Short-term treatments with REEs (minutes) have been classically used to block non-selective cation channels (Biagi and Enyeart, 1990; Lansman, 1990; Elinder and Arhem, 1994) and/or stretch-activated Ca²⁺-permeable channels at the PM (Yang and Sachs, 1989; Franco *et al.*, 1991; Hamill and McBride, 1996; Ermakov *et al.*, 2010), but recent studies have shown that long-term treatments with REEs promote their internalization and activate endocytosis in plant cells (L. Wang *et al.*, 2014, 2016, 2019). Here we show that the dynamics of the REE-induced EPCS reorganization are not consistent with the Ca²⁺ channel-blocking activity of REEs at the PM but rather is a consequence of their slow internalization to the cytosol. We also show that the EPCS-remodeling process is associated with the activation of the Ca²⁺ signaling in the cytosol, and the accumulation of phosphatidylinositol-4-phosphate (PI4P) at the PM.

Our results highlight commonalities between the EPCS remodeling triggered by REEs (this study) and NaCl (Lee *et al.*, 2019), such as the slow dynamics of the remodeling process and the concomitant accumulation of negatively charged phosphoinositides at the PM. These findings also uncover key differences such as the identity of the phosphoinositide species that are accumulated, PI4P for REEs (this study), and PI(4,5)P₂ for NaCl (Lee *et al.*, 2019), and the differential requirement for a functional cortical cytoskeleton for REE- and NaCl-induced EPCS remodeling. In a broader context, our study shows that the direct manipulation of extracellular Ca²⁺ levels has limited effects on plant EPCS organization, and supports a model where the slow accumulation of stress-specific phosphoinositide species at the PM acts as a general adaptive mechanism governing cortical ER–PM communication during sustained stress conditions.

Materials and methods

Plant materials and growth conditions

Arabidopsis thaliana Columbia (Col-0) was used as the wild type and the background for transgenes. Seeds of the mutants *sy1-1* (SALK_036961) and *clb1-2* (SALK_006298) were obtained from the Arabidopsis Biological Resource Center (Ohio State University). Previously published lines in this study are SYT1–green fluorescent protein (GFP) and MAPPER–GFP (Lee *et al.*, 2019); GFP–HDEL (Batoko *et al.*, 2000); 35S::C2AB (Pérez-Sancho *et al.*, 2015); GCaMP3 (DeFalco *et al.*, 2017); CITRINE-2×PH^{PLC}; and CITRINE 1×PH^{FAPP} (Simon *et al.*, 2016). Plants were grown on half-strength Murashige and Skoog (MS) medium (Caisson Labs) or soil (Sunshine mix #4, Sun Gro Horticulture Canada Ltd) at 22 °C with a 16 h light/8 h dark cycle. For the NaCl assays, Arabidopsis seedlings were grown vertically for 4 d on 1/10th strength MS medium, and similar sized seedlings were transferred to the same medium supplemented with different NaCl concentrations. The root elongation and root hair phenotypes were scored after 9 d.

Co-immunoprecipitation and large-scale immunoprecipitation for LC-MS/MS

Large-scale immunoprecipitation (IP) assays for LC-MS/MS were performed as described before (Kadota *et al.*, 2016), using 5–8 g of 10-day-old Arabidopsis seedlings stably expressing p35S:GFP (Lee *et al.*, 2019; Wang *et al.*, 2019). For targeted co-IPs, 1 g of 10-day-old Arabidopsis stable transgenic lines expressing p35S:GFP (control), pUB10:CLB1–GFP, and pSYT5:SYT5–GFP were used. Protein extraction buffer was (for both targeted and LC-MS/MS-coupled co-IP): 50 mM Tris–HCl pH 7.5, 150 mM NaCl, 10% glycerol, 10 mM EDTA, 1 mM Na₂MoO₄, 1 mM NaF, 0.5 mM Na₃VO₄, 10 mM DTT, 0.5 mM phenylmethylsulfonyl fluoride (PMSF), 1% (v/v) protease inhibitor cocktail, and 1% NP-40. Washing buffer was the same, but with only 0.2% NP-40. Total proteins were extracted by incubation with the extraction buffer for 40–50 min. IP was performed with GFP-Trap beads (Chromotek, Planegg-Martinsried, Germany). Proteins were stripped from the beads by boiling in 50 µl of SDS loading buffer for 20 min, vortexing regularly. Immunoprecipitated proteins were separated on SDS–PAGE acrylamide gels, and western blots were performed using anti-GFP (Santa Cruz Biotechnology sc-9996), anti-SYT1 (Pérez-Sancho *et al.*, 2015), anti-mouse IgG-peroxidase (Sigma A9044), and anti-rabbit IgG-peroxidase (Sigma A0545).

Molecular cloning and generation of transgenic plants

The *CLB1* and *SYT5* constructs used in this study were generated via PCR amplification using the reverse transcription–PCR (RT–PCR) product or genomic DNA as a template and gene-specific primers (Supplementary Table S2 at JXB online), followed by cloning PCR products into pENTR/TOPO (Invitrogen, Carlsbad, CA, USA) or pDONR221. To generate the *pUB10::CLB1-GFP* construct, the *CLB1* fragment was subcloned into the pB7m24GW,3 vector that contains a 615 bp UBQ10 promoter. To generate the p35S:SYT1–N–GFP, p35S:SYT1–C–GFP, p35S:SYT5–N–GFP, and p35S:SYT5–C–GFP constructs used in bimolecular fluorescence complementation (BiFC), combinations of pEN–L4–pro35S–R1 (Karimi *et al.*, 2007), pEN–L4–proSYT5–R1, pEN–R2–N–GFP–L3 (Boruc *et al.*, 2010), and pEN–R2–C–GFP–L3 (Boruc *et al.*, 2010) were recombined with pEN–L1–SYT1genomic–L2 (Pérez-Sancho *et al.*, 2015) and pEN–L1–SYT5genomic–L2 into pK7m34GW,0 (Karimi *et al.*, 2005). To generate the pCLB1::CLB1–GFP construct, the *CLB1* pENTR clone was recombined with the destination binary vector pGWB4. All resulting expression vectors were transformed in Arabidopsis via floral dip (Clough and Bent, 1998). The selection of transgenic lines was made on half-strength MS medium containing 25 µg ml^{−1} hygromycin (pGWB4) or 15 µg ml^{−1} glufosinate-ammonium (Sigma-Aldrich) (pB7m24GW,3).

Chemical applications

Chemicals were exogenously applied by incubating 5-day-old seedlings in liquid 1/10th strength MS medium and supplementing them with 500 µM LaCl₃ (Sigma-Aldrich), 500 µM GdCl₃ (Sigma-Aldrich), 5 mM EGTA (Sigma-Aldrich), or 25 µM oryzalin (Sigma-Aldrich) for 2 h or 16 h, or with 250 µM bis-(*o*-aminophenoxy) ethane-*N,N,N,N*-tetraacetic acid (BAPTA) (Sigma-Aldrich) or 1 µM latrunculin B (Abcam) for 2 h or 16 h. The duration of the treatments was based on the general toxicity caused by the different chemical compounds in plants. To visualize Hechtian strands, 5-day-old cotyledon epidermal cells expressing the different markers were plasmolyzed for 4 h using 0.4 M mannitol. The images are an overlay of propidium iodide-stained cell walls with the localization of the GFP fusion proteins in green.

Image acquisition and quantitative analyses

Living cell images were obtained using a Nikon C1 confocal laser scanning microscope, a Perkin-Elmer spinning disk confocal microscope, and an Olympus FV1000 multiphoton confocal laser scanning microscope. The Nikon C1 confocal laser scanning microscope was equipped with 488 nm and 515/30 nm emission filters and Nikon Plan Apochromat oil immersion objectives (×40, 1.0 NA and ×60, 1.4 NA, respectively). The Perkin-Elmer spinning disk confocal microscope was equipped with 488 nm and 561 nm lasers. The Olympus FV1000 was equipped with 405, 473, and 559 nm lasers and a ×60 oil Planon (×60, 1.4 NA). Images were captured using Nikon-EZ C1, Olympus FV1000, and Volocity software, respectively. To quantify the number of ‘beads’ configuration, 5-day-old Arabidopsis seedlings harboring the SYT1–GFP or SYT5–GFP marker were incubated for 16 h in liquid 1/10th strength MS medium (Mock) or liquid 1/10th strength MS medium supplemented with the different chemicals. For each treatment, the number of ‘beads’ labeled by SYT1–GFP or SYT5–GFP in the cortex of cotyledon epidermal cells was scored in at least 50 (15 µm×15 µm) regions of interest (ROIs) using the cell counter tool of Fiji (ImageJ) (National Institutes of Health, <http://imagej.nih.gov/ij/>) (Schindelin *et al.*, 2012). To compare the fluorescent intensity of the ratiometric CITRINE-1×PH^{FAPP} between control and treated samples, confocal laser scanning images of 5-day-old epidermal cotyledon cells were acquired from at least 10 individual seedlings. For each data point, the fluorescence intensity data were scored from at least 100 (15 µm×15 µm) ROIs using Fiji’s integrated density measurement tool (Schindelin *et al.*, 2012). In this analysis, stomatal lineage cells were excluded from the quantification. To compare the fluorescent intensity of the ratiometric GCaMP3 sensor, images of 5-day-old seedlings were acquired using a Nikon SMZ18 stereo microscope equipped with a 480/40 nm excitation filter, a Nikon P2-SHR Plan Apo ×0.5 objective, and a Nikon DS-Ri2 camera. The images were captured using NIS-Elements BR software version 4.60. For each data point, the fluorescence intensity data were scored from at least 50 seedlings. In the ratiometric analyses, the fluorescent data were normalized using the equation: $\Delta F/F = (F - F_0)/F_0$, where F_0 is the mean intensity of background fluorescence. The data were subject to one-way ANOVA to identify statistically significant differences among treatments. All statistical analyses were performed using the GraphPad Prism 5.0b software.

Accession numbers

The Arabidopsis Genome Initiative locus identifiers for genes used in this article are SYT1 (*At2g20990*), SYT5 (*At1g05500*), and CLB1 (*At3g61050*).

Results

SYT5 and *CLB1* are EPCS-localized proteins that interact with *SYT1* in vitro

SYT1 is a protein tether implicated in the establishment, organization, and function of plant EPCSs (Pérez-Sancho *et al.*, 2016a; Tilsner *et al.*, 2016; Bayer *et al.*, 2017; Wang *et al.*, 2017). Because the SYT1 orthologs in mammals [extended

synaptotagmins (E-Syts)] and yeast [tricalbins (Tcbs)] establish tethering complexes *in vivo* (Creutz *et al.*, 2004; Giordano *et al.*, 2013), we searched for additional proteins physically associated with Arabidopsis SYT1. For this purpose, we used a SYT1–GFP line in the *syt1-2* background (Lee *et al.*, 2019) and performed IP assays using agarose beads coupled to an anti-GFP nano-body (GFP–Trap beads). The IP results from three independent biological replicates provided a large number of proteins physically associated with SYT1 that we identified using LC–MS/MS. We filtered the results using the following criteria: (i) presence in all three biological replicates; (ii) detection of two or more exclusive unique peptides; and (iii) absence in the negative IP control (IP using a transgenic line expressing free GFP). After applying these filters, we identified two putative SYT1 interactors: Arabidopsis SYT5 (*At1g05500*; Ishikawa *et al.*, 2020) and CLB1/SYT7 (*At3g61050*; de Silva *et al.*, 2011; Ishikawa *et al.*, 2020) (Fig. 1A; Supplementary Table S1).

Bioinformatics analyses using Pfam (El-Gebali *et al.*, 2019) and TMHMM2 (Krogh *et al.*, 2001) databases show that SYT1, SYT5, and CLB1 share common domain architectures comprising a putative single N-terminal TM domain, an ~40 amino acid linker, a cytoplasm-exposed synaptotagmin-like mitochondrial lipid-binding protein (SMP) domain, and one (CLB1) or two (SYT1 and SYT5) phospholipid-binding C2 domains harboring lysine/arginine-rich (K/R-rich) polybasic patches (Fig. 1B; Supplementary Fig. S1). 3D modeling using Phyre2 (Kelley *et al.*, 2015) and 3DLigandSite (Wass *et al.*, 2010) shows that the predicted cytosolic regions of these proteins (SYT1_{30–541}, SYT5_{23–560}, and CLB1_{22–510}) can be modeled with >90% confidence using the crystal structure of the mammalian E-Syt2 as a template (Fig. 1C–E). The modeling also shows that SYT1, SYT5, and CLB1 contain a single Ca²⁺-binding site, whose position could be determined with confidence levels above the 99% threshold (Fig. 1C–E insets).

To assess the subcellular localization of the SYT5 and CLB1 proteins, we generated fluorescent SYT5–GFP and CLB1–GFP marker lines driven by their respective endogenous promoters. We used confocal microscopy and compared the SYT5–GFP and CLB1–GFP subcellular localization with that of the SYT1–GFP marker (Lee *et al.*, 2019). Figure 1F–Q shows that the SYT5–GFP and CLB1–GFP localization strongly resembles that of the SYT1–GFP marker in all tissues analyzed. These localizations include a ‘beads and strings’ arrangement in cotyledon epidermal cells (Fig. 1F–H), perinuclear labeling consistent with the ER in root meristematic cells (Fig. 1I–K), associations with the cell wall through Hechtian strands (Fig. 1L–N), and strong signal accumulation at root hair initiation sites (Fig. 1O–Q). The latter localization is consistent with a putative function for the SYT1/SYT5/CLB1 complex in root hair polarity maintenance, as indicated by the root hair phenotypes in the presence of NaCl of the *syt1/syt5/clb1* triple mutant (Supplementary Fig. S2). Although confocal microscopy alone is not sufficient to establish unequivocally whether the observed subcellular localizations represent EPCSs, the protein interaction data, the shared structural and functional features, and the common localization patterns strongly suggest that, like SYT1, SYT5 and CLB1 are enriched at EPCSs.

SYT1 and SYT5 establish homotypic and heterotypic interactions in vivo at EPCSs

To validate the interactions between SYT1, SYT5, and CLB1, we used a targeted co-IP assay using a previously reported anti-SYT1 polyclonal antibody (Pérez-Sancho *et al.*, 2015). For this experiment, we used the SYT1–GFP line in the *syt1-2* background (Lee *et al.*, 2019), a SYT1–GFP line in the Col background (Pérez-Sancho *et al.*, 2015), and we generated a transgenic line expressing SYT5–GFP under its native promoter (*SYT5::SYT5-GFP*) and a transgenic line expressing CLB1–GFP under a constitutive ubiquitin 10 promoter (*pUB10::CLB1-GFP*). Figure 2A and Supplementary Fig. S3 show that the affinity-purified SYT1–GFP was able to pull-down the native SYT1 (lane 1, 61.7 kDa band) from protein extracts *in vitro*, and that this interaction was not present when the SYT1–GFP line in the *syt1-2* background was used (lane 2). SYT5–GFP and CLB1–GFP were also able to pull-down the native SYT1 from protein extracts (lanes 4 and 5, 61.7 kDa band). Next, we assessed the putative interaction of these proteins *in vivo* using BiFC assays. Figure 2B–E shows that transient co-expression of different SYT1 and SYT5 BiFC constructs in *Nicotiana benthamiana* leaves render BiFC signals consistent with SYT1 and SYT5 interacting and forming homo- and heterodimers at PM subdomains. Despite multiple attempts, we failed to observe a BiFC signal between SYT1 and CLB1, and focused our subsequent analyses on SYT1 and SYT5. During the revision of this study, Ishikawa *et al.* (2020) reported the interaction between SYT1 and CLB1 *in vivo* using BiFC.

The putative SYT1/SYT5 EPCS complex is largely insensitive to extracellular Ca²⁺ depletion but relocalizes in response to internalization of REEs

The SYTs orthologs in yeast and mammals are Ca²⁺-responsive proteins that sense changes in [Ca²⁺]_{cyt} and regulate the non-vesicular transfer of signaling molecules between the cortical ER and the PM (Creutz *et al.*, 2004; Giordano *et al.*, 2013; Helle *et al.*, 2013; Prinz, 2014). Because SYT1, SYT5, and CLB1 contain a putatively conserved Ca²⁺-binding site in their 3D structure, we asked whether Ca²⁺ signals could influence the localization and dynamics of the SYT1/SYT5 tethering complex. To address this question, we first analyzed the effect of extracellular Ca²⁺ depletion on SYT1–GFP and SYT5–GFP localization using the extracellular Ca²⁺-chelating agents EGTA and BAPTA (Brault *et al.*, 2004; Nakagawa *et al.*, 2007) at different time points. In 2 h treatments, the depletion of free apoplasmic Ca²⁺ induced by either EGTA or BAPTA does not have a significant effect on the number of SYT1–GFP- and SYT5–GFP-labeled ‘beads’ at the cell cortex (Supplementary Fig. S4). In 16 h treatments, EGTA and BAPTA induced an ~1.5- to 1.8-fold increase in the number of SYT1–GFP- and SYT5–GFP-labeled ‘beads’ and a reduction in the average reticulate size of the cortical ER network (Fig. 3A–F, R). We also tested the effect of La³⁺ and Gd³⁺ REEs on SYT1–GFP and SYT5–GFP localization at different time points. Supplementary

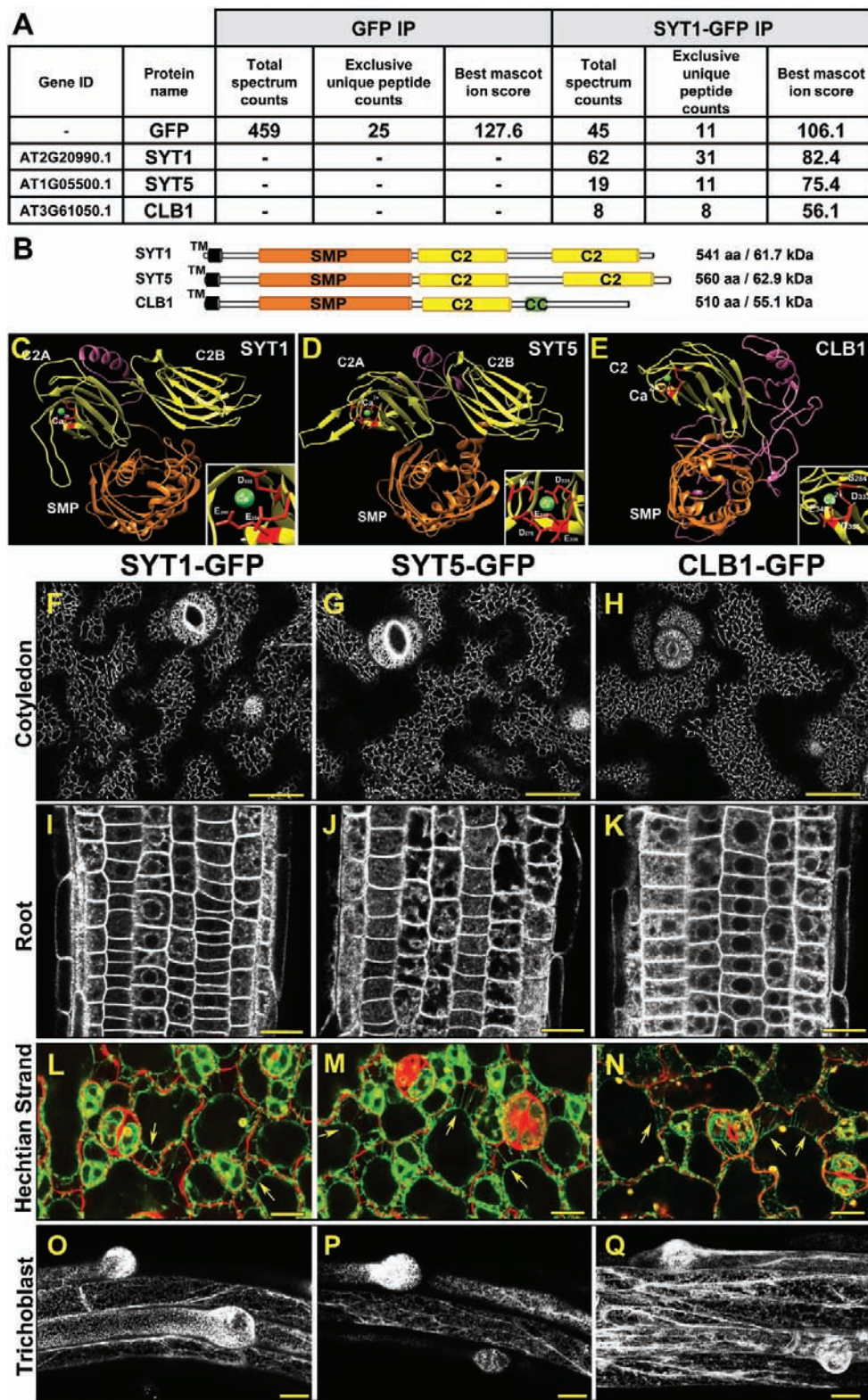


Fig. 1. The Ca²⁺-dependent phospholipid-binding proteins SYT5 and CLB1 interact with SYT1. (A) Peptide counts detected upon GFP immunoprecipitation followed by LC-MS/MS analysis using Arabidopsis plants expressing GFP (control) and SYT1-GFP. Numbers indicate the total spectrum counts corresponding to the indicated proteins, and the exclusive unique peptides represented within them. The best Mascot ion score among these peptides is indicated. The number of peptides corresponding to GFP is shown for reference. This result is representative of three independent experiments (for details on the replicates, see Supplementary Table S1). (B) Schematic representation of the functional domains of SYT1, SYT5, and CLB1. TM, transmembrane domain; SMP, synaptotagmin-like mitochondrial-lipid binding domain; C2, phospholipid-binding domains; CC, coiled-coil domain. (C–E) 3D structures and Ca²⁺-binding sites in the predicted cytosolic regions of SYT1 (C), SYT5 (D), and CLB1 (E) identified using Phyre2 and 3DLigand site. Important amino acid residues for Ca²⁺ binding are indicated in red. (F–Q) Subcellular localization of the SYT1-GFP, SYT5-GFP, and CLB1-GFP markers in epidermal cells of 5-day-old cotyledons (F–H), root meristematic cells of 5-day-old seedlings (I–K), Hechtian strands in plasmolyzed cells (L and M arrows), and emerging root hairs in 7-day-old seedlings (O–Q). Scale bars (F–K)=25 μ m; (L–M)=20 μ m; and (O–Q)=25 μ m.

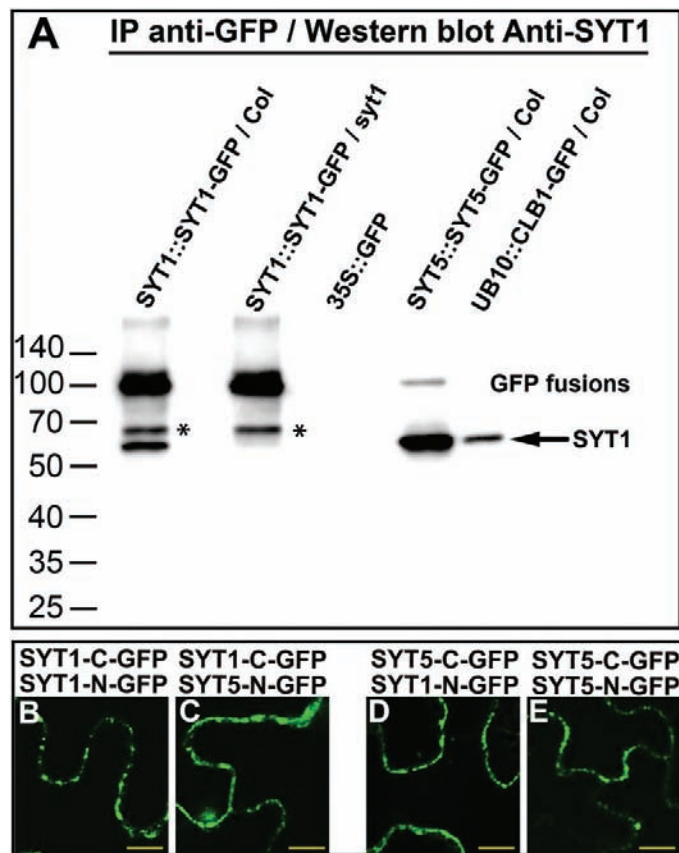


Fig. 2. SYT1 and SYT5 form homo- and heterodimeric complexes. (A) Arabidopsis transgenic plants expressing SYT1–GFP, SYT5–GFP, and CLB1–GFP were used for immunoprecipitation using GFP–Trap beads. Plants expressing free GFP were used as control. The immunoprecipitated proteins were separated by SDS–PAGE, and western blots were analyzed using anti-SYT1. Molecular weight (kDa) marker bands are indicated for reference. The arrow indicates the expected molecular weight for SYT1. *indicate a SYT1–GFP–derived fragment recognized by the SYT1 antibody. (B–E) BiFC analyses of SYT1/SYT5 interactions. *Nicotiana benthamiana* leaves were co-transformed transiently with the following SYT1 and SYT5 combinations: SYT1–C–GFP and SYT1–N–GFP (B), SYT1–C–GFP and SYT5–N–GFP (C), SYT5–C–GFP and SYT1–N–GFP (D), and SYT5–C–GFP and SYT5–N–GFP (E), and imaged after 4 d. Scale bars=10 μ m.

Fig. S5 shows that the Ca^{2+} channel-blocking activity of REEs in 30 min treatments did not induce changes in SYT1–GFP and SYT5–GFP localization. Remarkably, 2 h treatments induced a variable 2- to 4-fold increase in the number of SYT1–GFP- and SYT5–GFP-labeled ‘beads’ in individual epidermal cells (Supplementary Fig. S4), and 16 h treatments induced a generalized 4- to 5-fold increase in the number of SYT1–GFP- and SYT5–GFP-labeled ‘beads’ in all epidermal cells (Fig. 3J–Q). The treatment was associated with a significant reduction of the average reticule size of the cortical ER network (Fig. 3R), and with an increase in the number of ‘beads’ labeled by the artificial EPCS marker MAPPER–GFP (Lee *et al.*, 2019) (Supplementary Fig. S6). Remarkably, a 16 h La^{3+} treatment did not induce major changes in the localization of a truncated SYT1–GFP marker harboring the C2 phospholipid-binding domains (C2AB–GFP; Pérez-Sancho *et al.*, 2015) that is still homogeneously distributed at the PM (Supplementary Fig. S7).

The dynamics of SYT1–GFP and SYT5–GFP relocalization are consistent with EPCS remodeling being triggered by the slow internalization of REEs to the cytosol (L. Wang *et al.*, 2014, 2016, 2019). In this scenario, the addition of EGTA, a polydentate chelator that forms stable complexes with both Ca^{2+} and REEs (Tei *et al.*, 2010), should maintain REEs in the extracellular space and prevent the REE-induced SYT1–GFP and SYT5–GFP relocalization. Figure 4A–E shows that the supplementation of the REE treatments with 5 mM EGTA was sufficient to abolish the REE-induced SYT1–GFP relocalization in 16 h treatments, and reduce the long-term toxicity of the REEs in seedlings treated for 14 d (Supplementary Fig. S8). These results suggest that REE internalization, and not the blockage of extracellular Ca^{2+} entry induced by either REEs or Ca^{2+} chelators, underlies EPCS remodeling.

Internalized REEs can act as Ca^{2+} signaling surrogates in the cytosol

Biochemical studies have shown that REEs act as allosteric regulators of multiple Ca^{2+} -binding proteins *in vitro* (Mills and Johnson, 1985; Bertini *et al.*, 2003; Ye *et al.*, 2005; L. Wang *et al.*, 2016), so we asked whether internalized REEs could replace Ca^{2+} and mimic its effect *in vivo*. To answer this question, we analyzed the effect of REEs on the cytosolic activity of the calmodulin-based ratiometric Ca^{2+} sensor GCaMP3 (Tian *et al.*, 2009). Figure 5A–G shows that 16 h REE treatments that promote their internalization also induce a 2- to 3-fold increase in the GCaMP3 fluorescent signal in a process that is abolished by 5 mM EGTA supplementation. These results are consistent with internalized REEs acting as Ca^{2+} surrogates and binding proteins containing Ca^{2+} /calmodulin-like binding domains.

The La^{3+} -induced relocalization is cytoskeleton dependent and it is associated with PI4P accumulation at the PM

In the final experiment, we used 500 μM La^{3+} and 100 mM NaCl treatments for 16 h to explore whether the REE-induced EPCS reorganization is mechanistically similar to that previously reported for NaCl stress (Lee *et al.*, 2019). First, we tested whether the cortical cytoskeleton plays a role in the La^{3+} -induced EPCS remodeling. Our results show a differential behavior between the treatments as, compared with NaCl stress (Lee *et al.*, 2019), La^{3+} does not cause visible disruption of the cortical cytoskeleton network (Supplementary Fig. S9), and its effect on EPCS organization is partially abolished by pre-treatments with the microtubule-depolymerizing drug oryzalin or the actin polymerization inhibitor latrunculin B (Fig. 6A–N). Next, we tested whether the La^{3+} -induced EPCS remodeling was associated with the accumulation of phosphoinositides at the PM using the ratiometric sensors citrine $1\times\text{PH}^{\text{FAPP1}}$ (for PI4P) and $2\times\text{PH}^{\text{PLC}}$ [for PI(4,5) P_2] (Simon *et al.*, 2016). Our results show that 16 h La^{3+} treatments do not induce accumulations of the PI(4,5) P_2 sensor (Supplementary Fig. S10), but did induce an \sim 2-fold increase of the PI4P fluorescent signal at the PM (Fig. 7A, B, E). Remarkably, the 16 h

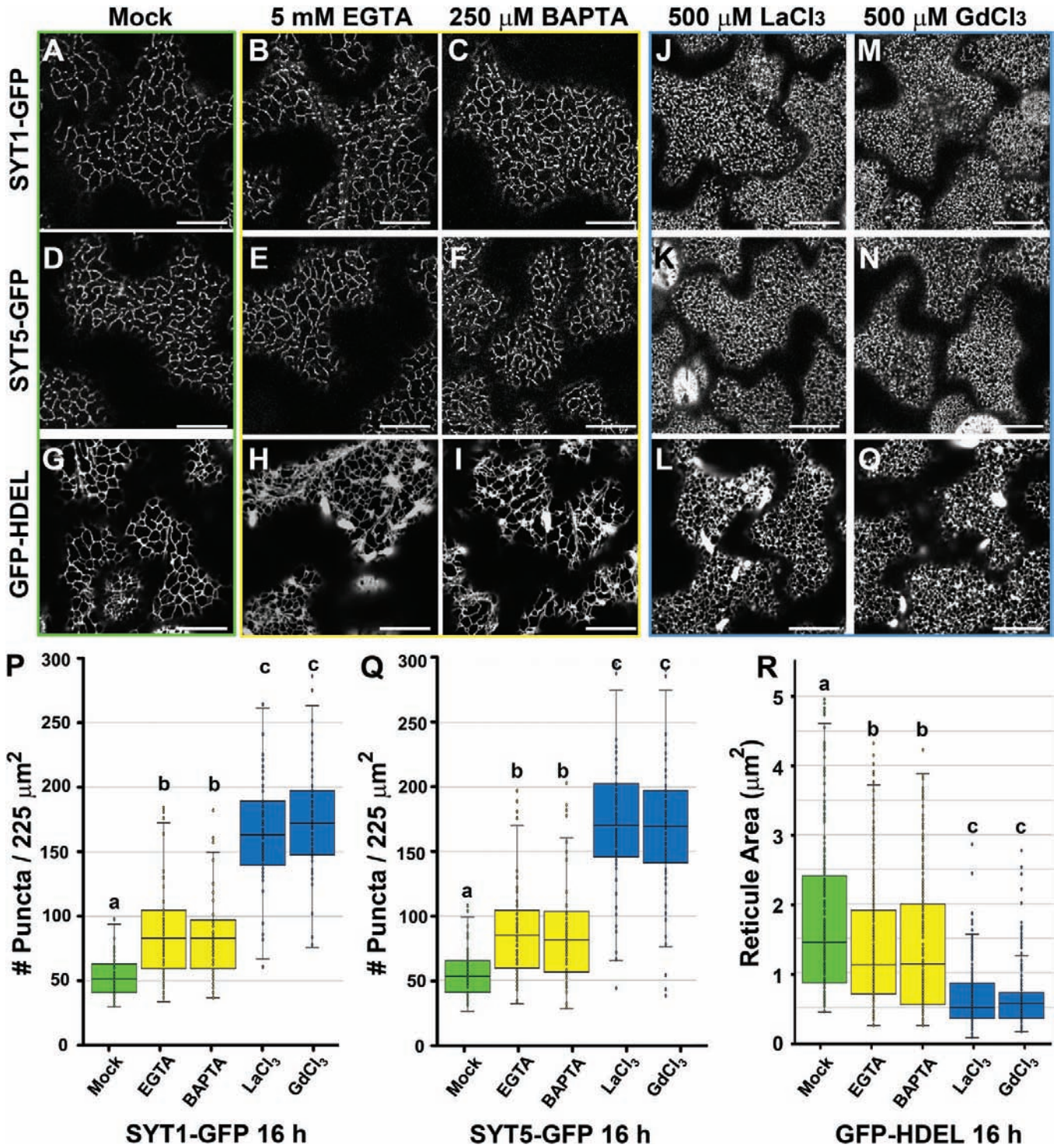


Fig. 3. Extracellular Ca²⁺ depletion and REE treatments increase the EPCS number and reduce cortical ER reticulation. Five-day-old SYT1-GFP, SYT5-GFP, and HDEL-GFP seedlings were treated in liquid 1/10th strength MS medium supplemented with Mock (A–C), EGTA (5 mM) (D–F), BAPTA (250 μM) (G–I), LaCl₃ (500 μM) (J–L), or GdCl₃ (500 μM) (M–O) for 16 h prior to imaging and quantification. (P and Q) Quantification of SYT1-GFP and SYT5-GFP puncta at the cell cortex upon chemical treatments. (R) Quantification of HDEL-GFP reticulation. In (P–R), the number of puncta or closed reticules was scored using 50–60 arbitrary 225 μm² ROIs from at least 15 cells from five independent seedlings. In the box and whiskers plots, the center line represents the median number of puncta or closed reticules per 225 μm², the top and bottom edges are the 25th and 75th percentiles of the distribution, and the ends of the whiskers are set at 1.5 times the interquartile range (IQR). All values outside the IQR are shown as outliers (dots). Letters indicate statistically significant differences using Tukey multiple pairwise comparisons $P < 0.05$. Scale bars = 20 μm.

La³⁺ treatment also induced the formation of PI4P-labeled vesicle-like structures closely associated with the PM (Fig. 7B asterisks). Consistent with previous findings, the addition of

5 mM EGTA to the extracellular medium was sufficient to inhibit the La³⁺-induced PI4P accumulation and the formation of PI4P vesicles (Fig. 7C, D). The results support a model

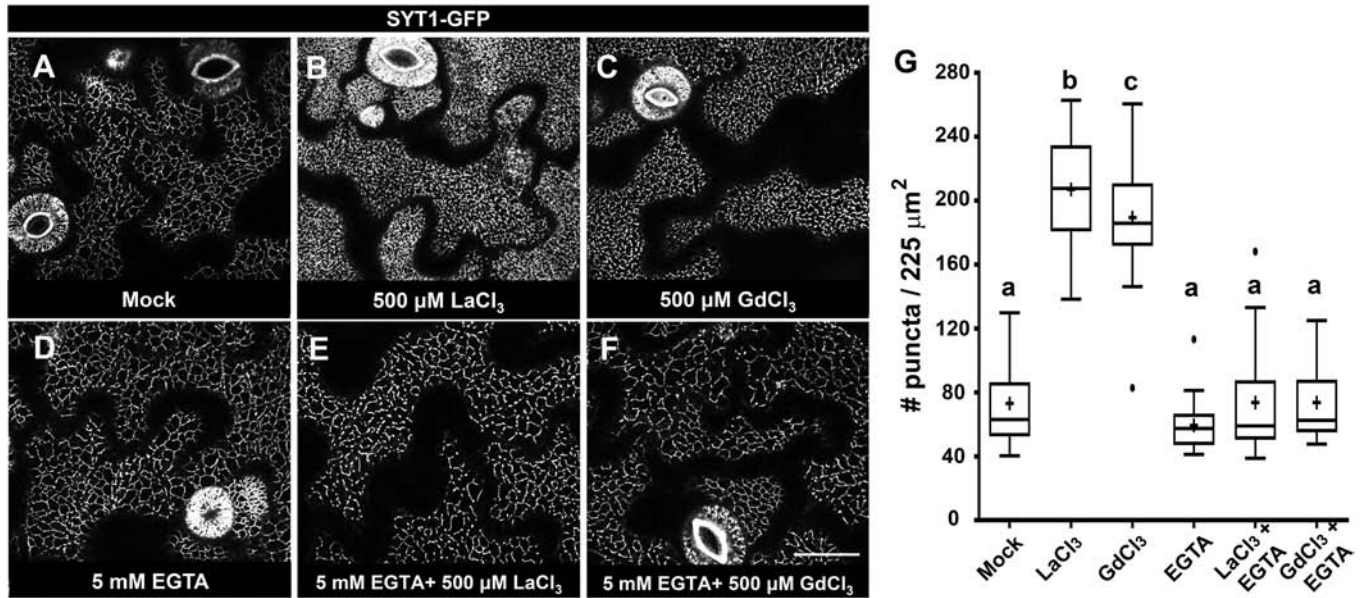


Fig. 4. The addition of EGTA to the growth medium reduces the SYT1-GFP and SYT5-GFP localization changes associated with REE internalization. Five-day-old SYT1-GFP seedlings were treated in liquid 1/10th strength MS medium supplemented with Mock (A), LaCl_3 (500 $\mu\text{M}/16$ h) (B) GdCl_3 (500 $\mu\text{M}/16$ h) (C), or the same medium supplemented with 5 mM EGTA (D–F) before imaging. (G) Quantification of the SYT1-GFP cortical signal. For each treatment, the number of puncta was scored using 50–60 arbitrary 225 μm^2 ROIs from at least 15 cells from five independent seedlings. In the box and whiskers plots, the center line represents the median number of puncta per 225 μm^2 , the top and bottom edges are the 25th and 75th percentiles of the distribution, and the ends of the whiskers are set at 1.5 times the interquartile range (IQR). When present, the minimum/maximum values outside the IQR are shown as outliers (dots). Letters indicate statistically significant differences using Tukey multiple pairwise comparisons $P < 0.05$. Scale bar = 20 μm .

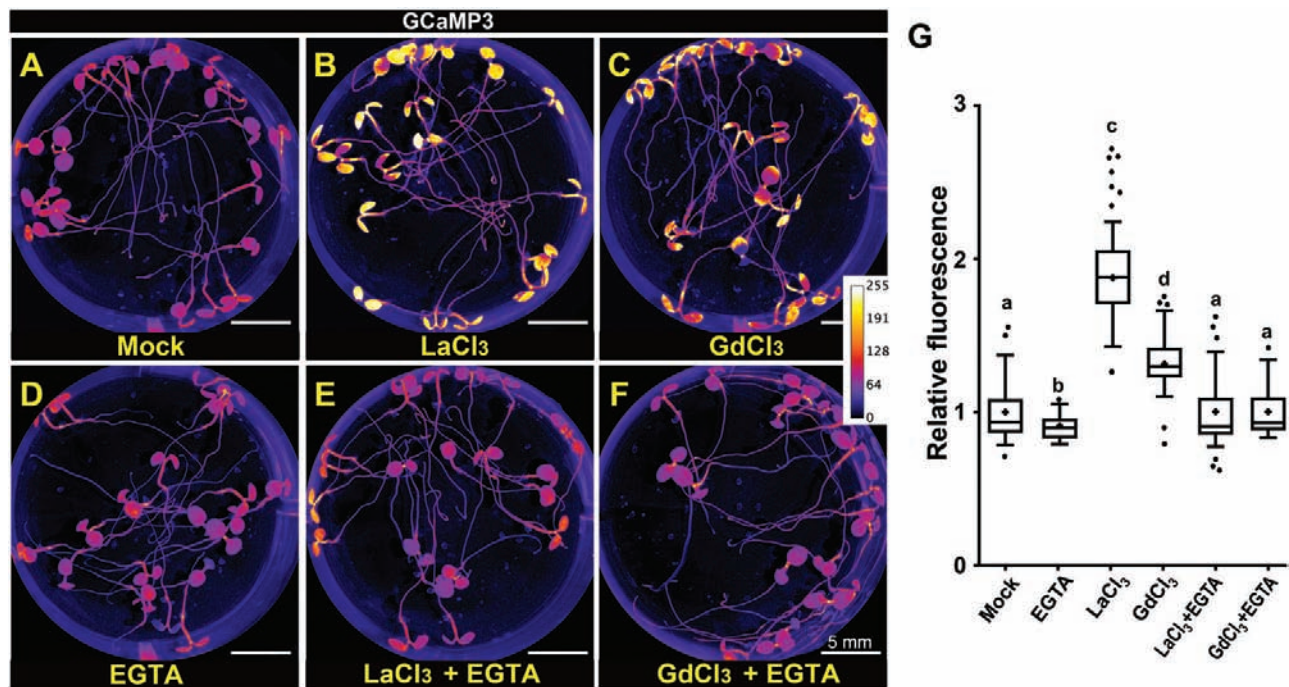


Fig. 5. REEs induce the activation of the cytosolic GCaMP3 Ca^{2+} sensor. Fluorescence images of seedlings expressing the GCaMP3 Ca^{2+} sensor. Five-day-old seedlings were treated in liquid 1/10th strength MS medium supplemented with Mock, 16 h (A), LaCl_3 (500 $\mu\text{M}/16$ h) (B), GdCl_3 (500 $\mu\text{M}/16$ h) (E), or the same medium supplemented with 5 mM EGTA (D–F). The activity of the Ca^{2+} sensor is shown as color-coded pixel intensity following the LUT scale shown in (F). (G) Quantification of the GCaMP3 signal relative to mock conditions. The center line represents the median fluorescence intensity fold increase relative to mock, the cross represents the mean fluorescent intensity, the top and bottom edges are the 25th and 75th percentiles of the distribution, and the ends of the whiskers are set at 1.5 times the interquartile range (IQR). All values outside the IQR are shown as outliers. The intensity of the signal was measured for at least 50 seedlings per treatment. Letters indicate statistically significant differences using Tukey multiple pairwise comparisons $P < 0.05$. Scale bar = 5 mm.

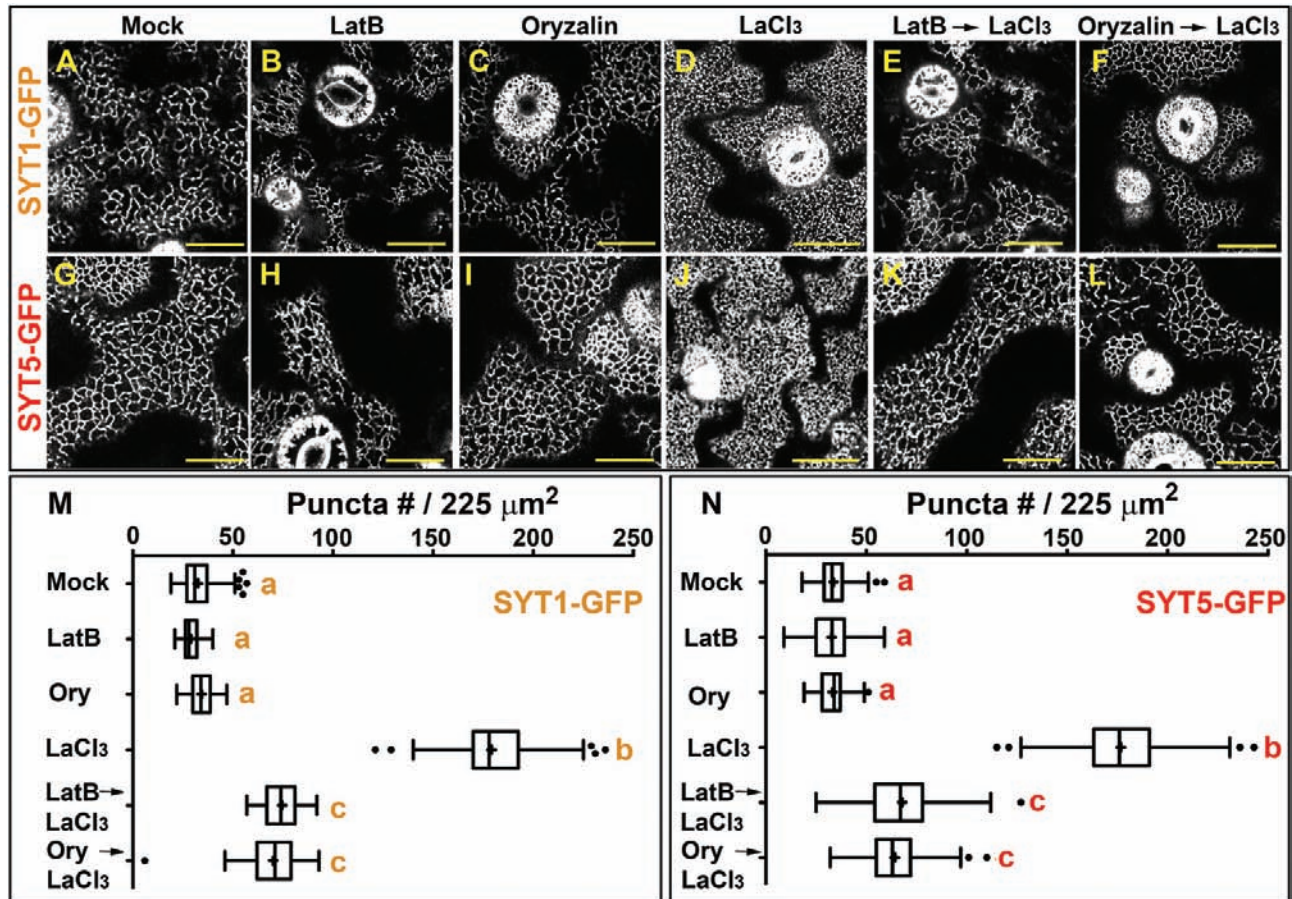


Fig. 6. REEs induce cytoskeleton-dependent changes in EPCS configuration. Confocal images of the cell cortex in cotyledon epidermal cells expressing the SYT1-GFP (A–F) and SYT5-GFP (G–L) markers. Five-day-old transgenic seedlings grown in 1/10th MS were transferred to liquid 1/10th MS for 16 h (A and G), or the same medium supplemented with LatB (1 μM, 2 h) (B and H), oryzalin (25 μM, 16 h) (C and I), LaCl₃ (500 μM, 16 h) (D and J), or sequentially treated with LatB (1 μM, 2 h) followed by LaCl₃ (500 μM, 16 h) (E and K) or oryzalin (25 μM, 16 h) followed by LaCl₃ (500 μM, 16 h) (F–L) before imaging. (M and N) Quantification of SYT1-GFP and SYT5-GFP puncta at the cell cortex upon chemical treatments. For each treatment, the number of SYT1-GFP and SYT5-GFP puncta was scored from 50–60 arbitrary 225 μm² ROIs from at least 15 cells from five different seedlings. In the box and whiskers plots, the center line represents the median number of puncta per 225 μm², the top and bottom edges are the 25th and 75th percentiles of the distribution, and the ends of the whiskers are set at 1.5 times the interquartile range (IQR). The minimum maximum values outside the IQR are shown as outliers (dots). Letters indicate statistically significant differences using Tukey multiple pairwise comparisons $P < 0.05$. Scale bars = 20 μm. (This figure is available in color at JXB online.)

where stress-induced accumulations of specific phosphoinositides is associated with either cytoskeleton-dependent or cytoskeleton-independent rearrangements of EPCS-localized protein complexes (Fig. 8).

Discussion

The plant EPCS responses to $[Ca^{2+}]_{cyt}$ are unique among eukaryotes

EPCSs are ubiquitous structures in eukaryotes, and they adopt distinct shapes and architectures in response to environmental and developmental cues. In mammals and yeast, EPCSs have a well-known role in the control of Ca^{2+} dynamics but, in plants, the presence of a cell wall that maintains a high extracellular Ca^{2+} concentration, and the presence of a complex suite of Ca^{2+} channels, transporters, and signaling components (Wheeler and Brownlee, 2008; De Vriese et al.,

2018) has limited our understanding of the role of Ca^{2+} in cortical ER–PM communication. Mammalian E-Syts and plant SYT1/SYT5 EPCS complexes share a common basic organization as both establish homotypic and heterotypic protein-tethering complexes with their N-terminal domains anchored to the ER, and their C-terminal C2 domains establishing Ca^{2+} -dependent interactions with the PM (Giordano et al., 2013; Pérez-Sancho et al., 2015; this study). Intriguingly, the mammalian E-Syts aggregate and concentrate at membrane junctions following a rise in $[Ca^{2+}]_{cyt}$ (Giordano et al., 2013), and this behavior is replicated by SYT1 in response to La^{3+} treatments. To explain this observation, Ishikawa et al. (2018) proposed that SYT1 responds to a decrease, instead of an increase, in $[Ca^{2+}]_{cyt}$ due to the activity of La^{3+} as a Ca^{2+} channel blocker at the PM. Our results reconcile this seemingly contrasting behavior in plants and mammals by showing that, in long-term treatments, internalized REEs are capable of triggering intracellular Ca^{2+}

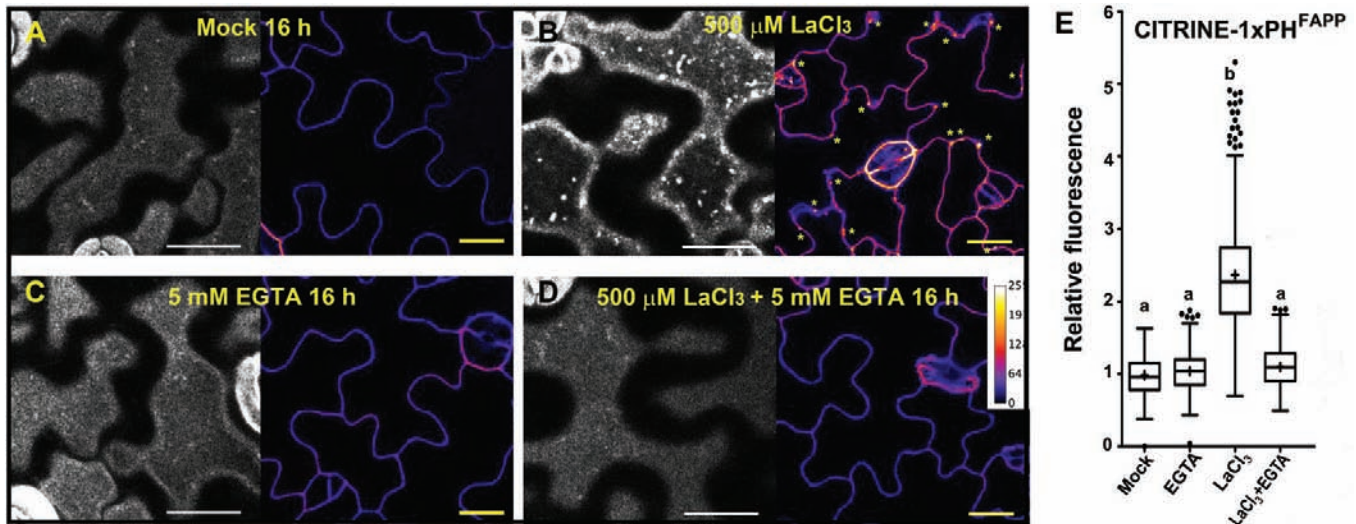


Fig. 7. La^{3+} induces the accumulation of PI4P at the PM and the formation of PI4P-containing vesicles. (A–D) Confocal images of the cell cortex and equatorial planes of cotyledon epidermal cells expressing the CITRINE-1 \times PH^{FAPP} marker. Five-day-old seedlings were treated in liquid 1/10th strength MS medium supplemented with Mock, 16 h (A), LaCl_3 (500 μM /16 h) (B), EGTA (5 mM/16 h) (C), or LaCl_3 (500 μM)+EGTA (5 mM)/16 h (D). The presence of PI4P-labeled vesicles is shown as bright dots at the PM (yellow asterisks). PI4P accumulation is shown as color-coded pixel intensity following the LUT scale shown in (D). (E) Quantification of the CITRINE-tagged 1 \times PH^{FAPP} signal relative to mock conditions. In the box plots, the center line represents the median fluorescence intensity fold increase relative to mock, the cross represents the mean fluorescent intensity, the top and bottom edges are the 25th and 75th percentiles of the distribution, and the ends of the whiskers are set at 1.5 times the interquartile range (IQR). All values outside the IQR are shown as outliers. At least 100 regions of interest (ROIs) were measured for each treatment. The letters indicate statistically significant differences using Tukey multiple pairwise comparisons $P < 0.05$. Scale bars = 20 μm .

signals, effectively offsetting their effect as PM Ca^{2+} channel blockers. Given that REEs can act as allosteric regulators of the activity of calmodulins (Mills and Johnson, 1985; L. Wang *et al.*, 2016), and C2-containing proteins *in vitro* (Essen *et al.*, 1997), we propose that internalized REEs could facilitate slow changes in ER–PM communication either by activating calmodulin signaling or through direct binding to the SYT1, SYT5, and/or CLB1 Ca^{2+} -binding domains *in vivo*.

The results discussed above highlight a clear difference in the temporal regulation of the Ca^{2+} -mediated responses between mammalian E-Syts and plant SYTs. In non-excitable mammalian cells, EPCSs control intracellular Ca^{2+} levels using store-operated Ca^{2+} entry (SOCE), a fast process that couples the Ca^{2+} influx from the extracellular space to the cytosolic Ca^{2+} release from the ER within seconds (Orci *et al.*, 2009). These mammalian cells can also sense high $[\text{Ca}^{2+}]_{\text{cyt}}$ and trigger the recruitment of E-Syt1 tethers to SOCE-independent EPCSs within minutes (Wu *et al.*, 2006). In contrast, the depletion of extracellular Ca^{2+} by chelating agents in Arabidopsis has limited effect on SYT1–GFP and SYT5–GFP localization, and EPCS remodeling in response to REEs and NaCl takes place within hours (this study; Lee *et al.*, 2019). Based on these observations, we hypothesize that the plant SYT1/SYT5 complexes are involved neither in the fast coupling of the extracellular and ER–lumen Ca^{2+} stores, nor in the fast response to $[\text{Ca}^{2+}]_{\text{cyt}}$ changes induced by stress. Instead, we propose that the observed EPCS remodeling in response to REEs is a consequence of the sensing and transduction of stress signals that promote long-term cellular adaptive responses, such as the slow changes in the PM lipid composition discussed in the next section.

Stress-specific regulatory mechanisms controlling EPCS organization in Arabidopsis

The cortical ER is a complex arrangement of tubules and small cisternae distributed towards the PM (Stefano *et al.*, 2014; Griffing *et al.*, 2017). EPCSs are important substructures within the cortical ER that can be defined as 200–300 nm long and 30 nm wide cortical ER nanodomains, which anchor to the PM using specialized tethering complexes (McFarlane *et al.*, 2017). In a differentiated plant cell, EPCSs can be localized in immobile ER tubules (Ishikawa *et al.*, 2018), and are associated with the cortical cytoskeleton (Peña and Heinlein, 2013; P. Wang *et al.*, 2014, 2016; Lee *et al.*, 2019). Currently, two functions of the cortical cytoskeleton array in EPCS establishment have been proposed. On the one hand, the actin and microtubule networks physically interact with VAP27/NET3C tethering complexes, fixing them on specific positions within the cell cortex (P. Wang *et al.*, 2014, 2016). This interaction might be required for cargo exchange during endocytic and exocytic trafficking (Peña and Heinlein, 2013; P. Wang *et al.*, 2014). On the other hand, the cortical cytoskeleton is required for the delivery of SYT1 tethers to EPCSs, and could also generate spatial incompatibility for EPCS establishment in regions where ‘thick’ cortical microtubules (25 nm in diameter) are closely associated with the PM (Pérez-Sancho *et al.*, 2015; McFarlane *et al.*, 2017; Lee *et al.*, 2019).

Given that SYT1/SYT5 complexes require a functional cortical cytoskeleton for proper reorganization in response to REEs, we hypothesize that their activity could be coordinated with that of the VAP27/NET3C EPCS complexes. In response to REE stress, the VAP27/NET3C and SYT1/SYT5 complexes could integrate cytoskeleton dynamics,

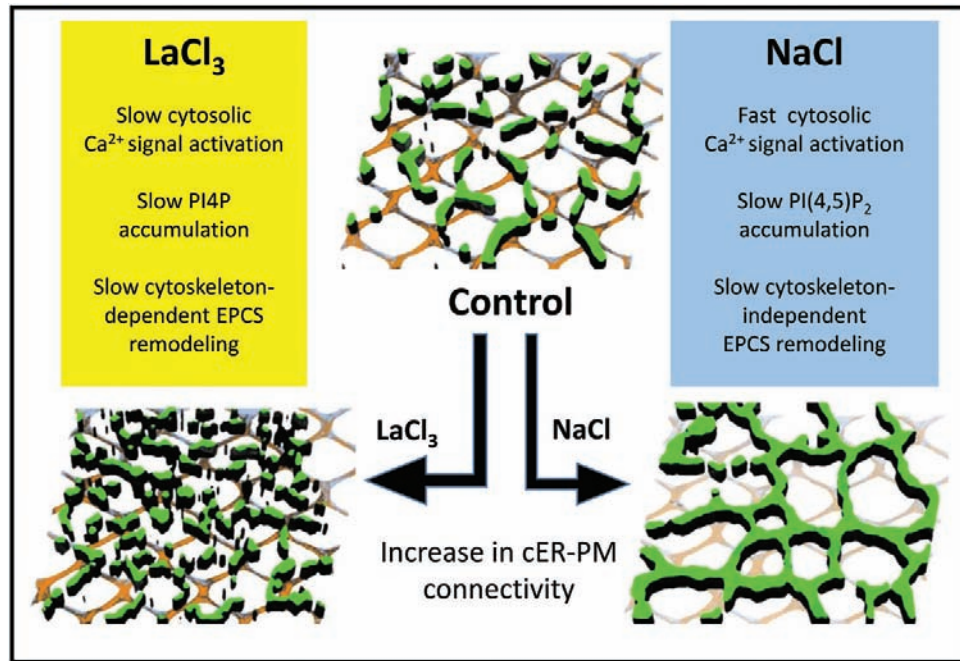


Fig. 8. Comparison of the mechanisms underlying LaCl_3 - and NaCl -induced EPCS remodeling. In this representation, the green signal represents the localization of the SYT1–GFP or SYT5–GFP markers at the cell cortex, and the crisscross pattern represents the cortical cytoskeleton.

cortical ER stability, and EPCS positioning, effectively controlling cortical ER–PM communication. In this context, the REE-induced PI4P accumulation at the PM could influence the electrostatic surface of the PM (Simon *et al.*, 2016), and regulate the docking affinity of the EPCS tethering complexes. Whether these changes in lipid composition could also activate endocytic and/or autophagic processes at EPCSs as proposed in Wang and Hussey (2019) has not been established and it is an area of active research in our laboratory. Remarkably, in plants subject to stress conditions that induce cytoskeleton disassembly (e.g. NaCl), an alternative SYT1-dependent mechanism promotes cytoskeleton-independent EPCS remodeling (Lee *et al.*, 2019). In these conditions, the NaCl -induced accumulation of $\text{PI}(4,5)\text{P}_2$ at the PM would have a minor influence on the PM electrostatic field, as PI4P still acts as the main contributor in this process (Simon *et al.*, 2016), but could fine-tune EPCS-associated signaling pathways acting as a substrate of PM-localized phospholipases (e.g. PI-PLCs) (Singh *et al.*, 2015). Together, these mechanisms illustrate the specificity and plasticity that govern EPCS rearrangements as an adaptive response to environmental stresses (Fig. 8).

Supplementary data

Supplementary data are available at *JXB* online.

Table S1. Unique peptide counts in three independent immunoprecipitation experiments.

Table S2. Primers used in this study.

Fig. S1. Multiple sequence alignment of the SYT1/SYT5/CLB1 C2 domains.

Fig. S2. Root hair polarization defects in the triple *syt1/syt5/club1* mutant.

Fig. S3. Expression control for immunoprecipitation experiments.

Fig. S4. Effect of 2 h extracellular Ca^{2+} depletion and REE treatments on EPCS number.

Fig. S5. Effect of short-term REE treatments on EPCS number.

Fig. S6. Effect of REE treatments on MAPPER–GFP localization.

Fig. S7. Effect of La^{3+} treatments on the localization of the PM marker C2AB–GFP.

Fig. S8. Effect EGTA supplementation on REE-induced seedling growth defects.

Fig. S9. Effect of NaCl and LaCl_3 treatments on cortical cytoskeleton organization.

Fig. S10. Effect of La^{3+} treatments on the accumulation of $\text{PI}(4,5)\text{P}_2$ at the PM.

Acknowledgements

This research was undertaken thanks to funding from the Natural Sciences and Engineering Research Council of Canada (NSERC) Discovery Grant RGPIN-2019-05568, the Canada Research Chairs program (to AR), and the Coordenação de Aperfeiçoamento de Pessoal de Nível Superior—Brasil (CAPES 88881.189854/2018-01, to BS).

References

- Andersson MX, Goksör M, Sandelius AS. 2007. Optical manipulation reveals strong attracting forces at membrane contact sites between endoplasmic reticulum and chloroplasts. *Journal of Biological Chemistry* **282**, 1170–1174.
- Barton K, Mathur N, Mathur J. 2013. Simultaneous live-imaging of peroxisomes and the ER in plant cells suggests contiguity but no luminal continuity between the two organelles. *Frontiers in Physiology* **4**, 196.

- Batoko H, Zheng HQ, Hawes C, Moore I.** 2000. A rab1 GTPase is required for transport between the endoplasmic reticulum and Golgi apparatus and for normal Golgi movement in plants. *The Plant Cell* **12**, 2201–2218.
- Bayer EM, Sparkes I, Vanneste S, Rosado A.** 2017. From shaping organelles to signalling platforms: the emerging functions of plant ER–PM contact sites. *Current Opinion in Plant Biology* **40**, 89–96.
- Bertini I, Gelis I, Katsaros N, Luchinat C, Provenzani A.** 2003. Tuning the affinity for lanthanides of calcium binding proteins. *Biochemistry* **42**, 8011–8021.
- Biagi BA, Enyeart JJ.** 1990. Gadolinium blocks low- and high-threshold calcium currents in pituitary cells. *American Journal of Physiology* **259**, C515–C520.
- Block MA, Jouhet J.** 2015. Lipid trafficking at endoplasmic reticulum–chloroplast membrane contact sites. *Current Opinion in Cell Biology* **35**, 21–29.
- Boruc J, Mylle E, Duda M, De Clercq R, Rombauts S, Geelen D, Hilson P, Inzé D, Van Damme D, Russinova E.** 2010. Systematic localization of the *Arabidopsis* core cell cycle proteins reveals novel cell division complexes. *Plant Physiology* **152**, 553–565.
- Brault M, Amiar Z, Pennarun AM, Monestiez M, Zhang Z, Cornel D, Dellis O, Knight H, Bouteau F, Rona JP.** 2004. Plasma membrane depolarization induced by abscisic acid in *Arabidopsis* suspension cells involves reduction of proton pumping in addition to anion channel activation, which are both Ca^{2+} dependent. *Plant Physiology* **135**, 231–243.
- Bravo-Sagua R, Torrealba F, Paredes F, et al.** 2014. Organelle communication: signaling crossroads between homeostasis and disease. *International Journal of Biochemistry and Cell Biology* **50**, 55–59.
- Clough SJ, Bent AF.** 1998. Floral dip: a simplified method for *Agrobacterium*-mediated transformation of *Arabidopsis thaliana*. *The Plant Journal* **16**, 735–743.
- Creutz CE, Snyder SL, Schulz TA.** 2004. Characterization of the yeast tricalbins: membrane-bound multi-C2-domain proteins that form complexes involved in membrane trafficking. *Cellular and Molecular Life Sciences* **61**, 1208–1220.
- Dalal J, Lewis DR, Tietz O, Brown EM, Brown CS, Palme K, Muday GK, Sederoff HW.** 2016. ROSY1, a novel regulator of gravitropic response is a stigmasterol binding protein. *Journal of Plant Physiology* **196–197**, 28–40.
- DeFalco TA, Toyota M, Phan V, Karia P, Moeder W, Gilroy S, Yoshioka K.** 2017. Using GCaMP3 to study Ca^{2+} signaling in *Nicotiana* species. *Plant & Cell Physiology* **58**, 1173–1184.
- de Silva K, Laska B, Brown C, Sederoff HW, Khodakovskaya M.** 2011. *Arabidopsis thaliana* calcium-dependent lipid-binding protein (AtCLB): a novel repressor of abiotic stress response. *Journal of Experimental Botany* **62**, 2679–2689.
- De Vriese K, Costa A, Beeckman T, Vanneste S.** 2018. Pharmacological strategies for manipulating plant Ca^{2+} signalling. *International Journal of Molecular Sciences* **19**, E1506.
- El-Gebali S, Mistry J, Bateman A, et al.** 2019. The Pfam protein families database in 2019. *Nucleic Acids Research* **47**, D427–D432.
- Elinder F, Arhem P.** 1994. Effects of gadolinium on ion channels in the myelinated axon of *Xenopus laevis*: four sites of action. *Biophysical Journal* **67**, 71–83.
- Ermakov YA, Kamaraju K, Sengupta K, Sukharev S.** 2010. Gadolinium ions block mechanosensitive channels by altering the packing and lateral pressure of anionic lipids. *Biophysical Journal* **98**, 1018–1027.
- Essen LO, Perisic O, Lynch DE, Katan M, Williams RL.** 1997. A ternary metal binding site in the C2 domain of phosphoinositide-specific phospholipase C- δ 1. *Biochemistry* **36**, 2753–2762.
- Fan J, Zhai Z, Yan C, Xu C.** 2015. *Arabidopsis* TRIGALAC TOSYLDIACYLGLYCEROL5 interacts with TGD1, TGD2, and TGD4 to facilitate lipid transfer from the endoplasmic reticulum to plastids. *The Plant Cell* **27**, 2941–2955.
- Franco A Jr, Winegar BD, Lansman JB.** 1991. Open channel block by gadolinium ion of the stretch-inactivated ion channel in mdx myotubes. *Biophysical Journal* **59**, 1164–1170.
- Giordano F, Saheki Y, Idevall-Hagren O, Colombo SF, Pirruccello M, Milosevic I, Gracheva EO, Bagriantsev SN, Borgese N, De Camilli P.** 2013. $\text{PI}(4,5)\text{P}_2$ -dependent and Ca^{2+} -regulated ER–PM interactions mediated by the extended synaptotagmins. *Cell* **153**, 1494–1509.
- Griffing LR, Lin C, Perico C, White RR, Sparkes I.** 2017. Plant ER geometry and dynamics: biophysical and cytoskeletal control during growth and biotic response. *Protoplasma* **254**, 43–56.
- Hamill OP, McBride DW Jr.** 1996. The pharmacology of mechanogated membrane ion channels. *Pharmacological Reviews* **48**, 231–252.
- Helle SC, Kanfer G, Kolar K, Lang A, Michel AH, Kornmann B.** 2013. Organization and function of membrane contact sites. *Biochimica et Biophysica Acta* **1833**, 2526–2541.
- Ho CM, Paciorek T, Abrash E, Bergmann DC.** 2016. Modulators of stomatal lineage signal transduction alter membrane contact sites and reveal specialization among ERECTA kinases. *Developmental Cell* **38**, 345–357.
- Ishikawa K, Tamura K, Fukao Y, Shimada T.** 2020. Structural and functional relationships between plasmodesmata and plant endoplasmic reticulum–plasma membrane contact sites consisting of three synaptotagmins. *New Phytologist* **226**, 798–808.
- Ishikawa K, Tamura K, Ueda H, Ito Y, Nakano A, Hara-Nishimura I, Shimada T.** 2018. Synaptotagmin-associated endoplasmic reticulum–plasma membrane contact sites are localized to immobile ER tubules. *Plant Physiology* **178**, 641–653.
- Kadota Y, Macho AP, Zipfel C.** 2016. Immunoprecipitation of plasma membrane receptor-like kinases for identification of phosphorylation sites and associated proteins. *Methods in Molecular Biology* **1363**, 133–144.
- Karimi M, De Meyer B, Hilson P.** 2005. Modular cloning in plant cells. *Trends in Plant Science* **10**, 103–105.
- Karimi M, Depicker A, Hilson P.** 2007. Recombinational cloning with plant gateway vectors. *Plant Physiology* **145**, 1144–1154.
- Kelley LA, Mezulis S, Yates CM, Wass MN, Sternberg MJ.** 2015. The Phyre2 web portal for protein modeling, prediction and analysis. *Nature Protocols* **10**, 845–858.
- Kim H, Kwon H, Kim S, Kim MK, Botella MA, Yun HS, Kwon C.** 2016. Synaptotagmin 1 negatively controls the two distinct immune secretory pathways to powdery mildew fungi in *Arabidopsis*. *Plant & Cell Physiology* **57**, 1133–1141.
- Kriechbaumer V, Botchway SW, Slade SE, Knox K, Frigerio L, Oparka K, Hawes C.** 2015. Reticulomics: protein–protein interaction studies with two plasmodesmata-localized reticulon family proteins identify binding partners enriched at plasmodesmata, endoplasmic reticulum, and the plasma membrane. *Plant Physiology* **169**, 1933–1945.
- Krogh A, Larsson B, von Heijne G, Sonnhammer EL.** 2001. Predicting transmembrane protein topology with a hidden Markov model: application to complete genomes. *Journal of Molecular Biology* **305**, 567–580.
- Lansman JB.** 1990. Blockade of current through single calcium channels by trivalent lanthanide cations. Effect of ionic radius on the rates of ion entry and exit. *Journal of General Physiology* **95**, 679–696.
- Lee E, Vanneste S, Pérez-Sancho J, Benitez-Fuente F, Strelau M, Macho AP, Botella MA, Friml J, Rosado A.** 2019. Ionic stress enhances ER–PM connectivity via phosphoinositide-associated SYT1 contact site expansion in *Arabidopsis*. *Proceedings of the National Academy of Sciences, USA* **116**, 1420–1429.
- Levy A, Zheng JY, Lazarowitz SG.** 2015. Synaptotagmin SYTA forms ER–plasma membrane junctions that are recruited to plasmodesmata for plant virus movement. *Current Biology* **25**, 2018–2025.
- Lewis JD, Lazarowitz SG.** 2010. *Arabidopsis* synaptotagmin SYTA regulates endocytosis and virus movement protein cell-to-cell transport. *Proceedings of the National Academy of Sciences, USA* **107**, 2491–2496.
- McFarlane HE, Lee EK, van Bezouwen LS, Ross B, Rosado A, Samuels AL.** 2017. Multiscale structural analysis of plant ER–PM contact sites. *Plant & Cell Physiology* **58**, 478–484.
- Michaud M, Gros V, Tardif M, et al.** 2016. AtMic60 is involved in plant mitochondria lipid trafficking and is part of a large complex. *Current Biology* **26**, 627–639.
- Mills JS, Johnson JD.** 1985. Metal ions as allosteric regulators of calmodulin. *Journal of Biological Chemistry* **260**, 15100–15105.
- Nakagawa Y, Katagiri T, Shinozaki K, et al.** 2007. *Arabidopsis* plasma membrane protein crucial for Ca^{2+} influx and touch sensing in roots. *Proceedings of the National Academy of Sciences, USA* **104**, 3639–3644.
- Orci L, Ravazzola M, Le Coadic M, Shen WW, Demaurex N, Cosson P.** 2009. STIM1-induced precortical and cortical subdomains of the endoplasmic reticulum. *Proceedings of the National Academy of Sciences, USA* **106**, 19358–19362.

- Peña EJ, Heinlein M.** 2013. Cortical microtubule-associated ER sites: organization centers of cell polarity and communication. *Current Opinion in Plant Biology* **16**, 764–773.
- Pérez-Sancho J, Schapire AL, Botella MA, Rosado A.** 2016b. Analysis of protein–lipid interactions using purified C2 domains. *Methods in Molecular Biology* **1363**, 175–187.
- Pérez-Sancho J, Tilsner J, Samuels AL, Botella MA, Bayer EM, Rosado A.** 2016a. Stitching organelles: organization and function of specialized membrane contact sites in plants. *Trends in Cell Biology* **26**, 705–717.
- Pérez-Sancho J, Vanneste S, Lee E, McFarlane HE, Esteban Del Valle A, Valpuesta V, Friml J, Botella MA, Rosado A.** 2015. The Arabidopsis synaptotagmin1 is enriched in endoplasmic reticulum–plasma membrane contact sites and confers cellular resistance to mechanical stresses. *Plant Physiology* **168**, 132–143.
- Prinz WA.** 2014. Bridging the gap: membrane contact sites in signaling, metabolism, and organelle dynamics. *Journal of Cell Biology* **205**, 759–769.
- Schapire AL, Voigt B, Jasik J, et al.** 2008. Arabidopsis synaptotagmin 1 is required for the maintenance of plasma membrane integrity and cell viability. *The Plant Cell* **20**, 3374–3388.
- Schindelin J, Arganda-Carreras I, Frise E, et al.** 2012. Fiji: an open-source platform for biological-image analysis. *Nature Methods* **9**, 676–682.
- Siao W, Wang P, Voigt B, Hussey PJ, Baluska F.** 2016. Arabidopsis SYT1 maintains stability of cortical endoplasmic reticulum networks and VAP27-1-enriched endoplasmic reticulum–plasma membrane contact sites. *Journal of Experimental Botany* **67**, 6161–6171.
- Simon ML, Platre MP, Marqués-Bueno MM, Armengot L, Stanislas T, Bayle V, Caillaud MC, Jaillais Y.** 2016. A PtdIns(4)P-driven electrostatic field controls cell membrane identity and signalling in plants. *Nature Plants* **2**, 16089.
- Singh A, Bhatnagar N, Pandey A, Pandey GK.** 2015. Plant phospholipase C family: regulation and functional role in lipid signaling. *Cell Calcium* **58**, 139–146.
- Sparkes IA, Ketelaar T, de Ruijter NC, Hawes C.** 2009. Grab a Golgi: laser trapping of Golgi bodies reveals in vivo interactions with the endoplasmic reticulum. *Traffic* **10**, 567–571.
- Stefano G, Hawes C, Brandizzi F.** 2014. ER—the key to the highway. *Current Opinion in Plant Biology* **22**, 30–38.
- Tei L, Baranyai Z, Brücher E, Cassino C, Demicheli F, Masciocchi N, Giovenzana GB, Botta M.** 2010. Dramatic increase of selectivity for heavy lanthanide(III) cations by tuning the flexibility of polydentate chelators. *Inorganic Chemistry* **49**, 616–625.
- Tian L, Hires SA, Mao T, et al.** 2009. Imaging neural activity in worms, flies and mice with improved GCaMP calcium indicators. *Nature Methods* **6**, 875–881.
- Tilsner J, Nicolas W, Rosado A, Bayer EM.** 2016. Staying tight: plasmodesmal membrane contact sites and the control of cell-to-cell connectivity in plants. *Annual Review of Plant Biology* **67**, 337–364.
- Uchiyama A, Shimada-Beltran H, Levy A, Zheng JY, Javia PA, Lazarowitz SG.** 2014. The Arabidopsis synaptotagmin SYTA regulates the cell-to-cell movement of diverse plant viruses. *Frontiers in Plant Science* **5**, 584.
- Wang L, Cheng M, Chu Y, Li X, Chen DDY, Huang X, Zhou Q.** 2016. Responses of plant calmodulin to endocytosis induced by rare earth elements. *Chemosphere* **154**, 408–415.
- Wang L, Cheng M, Yang Q, et al.** 2019. Arabinogalactan protein–rare earth element complexes activate plant endocytosis. *Proceedings of the National Academy of Sciences, USA* **116**, 14349–14357.
- Wang L, Li J, Zhou Q, et al.** 2014. Rare earth elements activate endocytosis in plant cells. *Proceedings of the National Academy of Sciences, USA* **111**, 12936–12941.
- Wang P, Hawes C, Hussey PJ.** 2017. Plant endoplasmic reticulum–plasma membrane contact sites. *Trends in Plant Science* **22**, 289–297.
- Wang P, Hawkins TJ, Richardson C, Cummins I, Deeks MJ, Sparkes I, Hawes C, Hussey PJ.** 2014. The plant cytoskeleton, NET3C, and VAP27 mediate the link between the plasma membrane and endoplasmic reticulum. *Current Biology* **24**, 1397–1405.
- Wang P, Hussey PJ.** 2019. Plant ER–PM contact sites in endocytosis and autophagy: does the local composition of membrane phospholipid play a role? *Frontiers in Plant Science* **10**, 23.
- Wang P, Richardson C, Hawkins TJ, Sparkes I, Hawes C, Hussey PJ.** 2016. Plant VAP27 proteins: domain characterization, intracellular localization and role in plant development. *New Phytologist* **210**, 1311–1326.
- Wang Y, Li Y, Rosas-Diaz T, Caceres-Moreno C, Lozano-Duran R, Macho AP.** 2019. The IMMUNE-ASSOCIATED NUCLEOTIDE-BINDING 9 protein is a regulator of basal immunity in *Arabidopsis thaliana*. *Molecular Plant–Microbe Interactions* **32**, 65–75.
- Wass MN, Kelley LA, Sternberg MJ.** 2010. 3DLigandSite: predicting ligand-binding sites using similar structures. *Nucleic Acids Research* **38**, W469–W473.
- Wheeler GL, Brownlee C.** 2008. Ca²⁺ signalling in plants and green algae—changing channels. *Trends in Plant Science* **13**, 506–514.
- Wu MM, Buchanan J, Luik RM, Lewis RS.** 2006. Ca²⁺ store depletion causes STIM1 to accumulate in ER regions closely associated with the plasma membrane. *Journal of Cell Biology* **174**, 803–813.
- Xu C, Fan J, Cornish AJ, Benning C.** 2008. Lipid trafficking between the endoplasmic reticulum and the plastid in Arabidopsis requires the extraplastidic TGD4 protein. *The Plant Cell* **20**, 2190–2204.
- Yamazaki T, Kawamura Y, Minami A, Uemura M.** 2008. Calcium-dependent freezing tolerance in Arabidopsis involves membrane resealing via synaptotagmin SYT1. *The Plant Cell* **20**, 3389–3404.
- Yamazaki T, Takata N, Uemura M, Kawamura Y.** 2010. Arabidopsis synaptotagmin SYT1, a type I signal-anchor protein, requires tandem C2 domains for delivery to the plasma membrane. *Journal of Biological Chemistry* **285**, 23165–23176.
- Yang XC, Sachs F.** 1989. Block of stretch-activated ion channels in *Xenopus* oocytes by gadolinium and calcium ions. *Science* **243**, 1068–1071.
- Ye Y, Lee HW, Yang W, Shealy S, Yang JJ.** 2005. Probing site-specific calmodulin calcium and lanthanide affinity by grafting. *Journal of the American Chemical Society* **127**, 3743–3750.